# Impact of a human gut microbe on *Vibrio cholerae* host colonization through biofilm enhancement

Kelsey Barrasso[1,2], Denise Chac[3], Meti D. Debela[6], Catherine Geigel[4], Jason B. Harris[6,7], Regina C. LaRocque[6], Firas S. Midani[8], Firdausi Qadri[9], Jing Yan[4,5], Ana A. Weil[3,*], Wai-Leung Ng[1,2,*]

**Affiliations:**

1. Department of Molecular Biology and Microbiology, Tufts University School of Medicine, Boston, MA
2. Program of Molecular Microbiology, Graduate School of Biomedical Sciences, Tufts University School of Medicine, Boston, MA
3. Department of Medicine, University of Washington, Seattle, WA
4. Department of Molecular, Cellular and Developmental Biology, Yale University, New Haven, CT
5. Quantitative Biology Institute, Yale University, New Haven, CT
6. Division of Infectious Diseases, Massachusetts General Hospital, Boston, MA
7. Department of Pediatrics, Harvard Medical School, Boston, MA
8. Department of Molecular Virology and Microbiology at Baylor College of Medicine, Houston, TX
9. International Center for Diarrheal Disease Research, Bangladesh, Dhaka, Bangladesh

* Co-corresponding authors/equal contributions

Corresponding authors: Ana A. Weil and Wai-Leung Ng

**Email:** anaweil@uw.edu wai-leung.ng@tufts.edu

**Author Contributions:**

- Designed research (KB, DC, JY, AAW, WLN)
- Performed research (KB, DC, MDD, CG, JY)
- Contributed new reagents or analytic tools (FSM, JY, JBH, RCL, FQ)
- Analyzed data (KB, DC, FSM, JY, AAW, WLN)
- Wrote the paper (KB, DC, JY, AAW, WLN)

**Competing Interest Statement:** No competing interests.

**Keywords:** Bacterial pathogenesis, gut microbiome, mixed species biofilm

## Abstract

Recent studies indicate that the human intestinal microbiota could impact the outcome of infection by *Vibrio cholerae,* the etiological agent of the diarrheal disease cholera. A commensal bacterium, *Paracoccus aminovorans,* was previously identified in high abundance in stool collected from individuals infected with *V. cholerae* when compared to stool from uninfected persons. However, if and how *P. aminovorans* interacts with *V. cholerae* has not been experimentally determined; moreover, whether any association between this bacterium alters the behaviors of *V. cholerae* to affect the disease outcome is unclear. Here we show that *P. aminovorans* and *V. cholerae* together form dual-species biofilm structures at the air-liquid interface, with previously uncharacterized novel features. Importantly, the presence of *P. aminovorans* within the murine small intestine enhances *V. cholerae* colonization in the same niche that is dependent on the *Vibrio* exopolysaccharide (VPS) and other major components of mature *V. cholerae* biofilm. These studies illustrate that dual-

species biofilm formation is a plausible mechanism used by a gut microbe to increase the virulence of the pathogen, and this interaction may alter outcomes in enteric infections.

**Significance Statement**

While ample evidence suggests that the outcome of some enteric infections can be affected by the intestinal microbiota, how specific gut microbes change the behaviors of a pathogen is unclear. Here we characterize the interaction between *Vibrio cholerae* and *Paracoccus aminovorans*, a gut microbe known to increase in abundance in the intestines during active *V. cholerae* infection in humans. These two bacteria form a dual-species biofilm structure at the air-liquid interface, and the gut microbe increases the host colonization efficiency of *V. cholerae*. Importantly, our study identifies a previously unknown mechanism of gut microbe-pathogen interaction that has the potential to alter the disease outcome.

61 **Introduction**

62 *Vibrio cholerae* (*Vc*) causes an estimated 3 million infections and 120,000 deaths each year, and
63 larger and more deadly outbreaks have increased during the last decade (1, 2). A wide range of
64 clinical outcomes occur in persons exposed to *Vc*, ranging from asymptomatic infection to severe
65 secretory diarrhea. It is nearly certain that many behaviors of *Vc* in the aquatic environment and
66 inside the host are significantly affected by the presence of other microbes (3), and recent studies
67 provide evidence that the gut microbiota may impact the severity of cholera (4-7).

68

69 Several functions of the gut microbiota influence the growth or colonization of enteric pathogens,
70 including production of anti-microbial compounds, maintenance of the intestinal barrier, regulation
71 of the host immune response, and modulation of available nutrients (8). Gut microbes have been
72 shown to have an important role in *Vc* infection in various animal models. For instance, disruption
73 of the commensal microbiota with antibiotics is required to allow successful *Vc* colonization in adult
74 rodent models (9, 10). Conversely, *Vc* actively employs a Type VI secretion system to attack host
75 commensal microbiota to enhance colonization of the gut in infant mice (11). Moreover, specific
76 microbial species have a profound impact on *Vc* colonization. *Blautia obeum*, an anaerobic Gram-
77 positive bacterium, decreases *Vc* intestinal colonization presumably by producing a signaling
78 molecule that induces *Vc* into a high cell-density quorum sensing state (5) in which virulence gene
79 expression is repressed (12, 13). Certain microbiota species reduce *Vc* colonization by producing
80 the enzyme bile salt hydrolase that degrades the host-produced virulence-activating compound
81 taurocholate (4, 5). Through metabolizing host glycans into short chain fatty acids that suppresses
82 *Vc* growth, a prominent commensal species, *Bacteroides vulgatus,* reduces *Vc* proliferation within
83 the intestine (14).

84

85 While the above studies exemplify how a single microbe or a group of microbes can protect the
86 host from *Vc* infection, the mechanisms used by certain gut microbes to promote *Vc* virulence,
87 thereby increasing the likelihood of individuals to develop cholera and worsen disease outcomes,

88 are less well understood. We have previously studied household contacts of cholera patients to
89 understand how gut microbes impact on susceptibility to cholera and identified bacteria associated
90 with increased or decreased susceptibility to *Vc* infection (6, 7). We also observed that the gut
91 microbial species *Paracoccus aminovorans* (*Pa*) was more likely to be present and more abundant
92 in the gut microbiota during *Vc* infection (7). The association between *Pa* and *Vc* is highly unusual
93 because most of the native gut microbiota is typically displaced by secretory diarrhea during cholera
94 (5, 15). To determine the underlying mechanisms driving these correlative clinical findings, we
95 evaluated the relationship between *Pa* and *Vc* in co-culture and determined the effects of *Pa* on *Vc*
96 infection outcomes with *in vivo* models. Here we show that *Pa* interacts directly with *Vc* to form
97 dual-species biofilm structures with previously uncharacterized features. Moreover, *Vc* colonization
98 inside the animal host is enhanced by the presence of *Pa* in the small intestine, and this effect is
99 dependent upon *Vc* biofilm production. Our findings demonstrate a plausible mechanism by which
100 a gut microbe specifically associates with *Vc,* and this reinforces our microbiome analysis in
101 humans that identified *Pa* as highly associated with infected individuals. Our findings also
102 demonstrate that interactions between these two species have the potential to directly impact *Vc*
103 pathogenesis and alter outcomes of *Vc* infection in humans.

104

105

106 **Results**

107 ***P. aminovorans* is differentially abundant in individuals with active *V. cholerae* infection**

108 *Paracoccus* is a genus of soil microbes found in low abundance in the gut microbiome of humans
109 (16, 17). Our previously published analysis of stool gut microbes from household contacts of
110 cholera patients identified *P. aminovorans (Pa*) as an unexpectedly abundant gut microbe during
111 active *V. cholerae* (*Vc*) infection, and this organism was rarely found in uninfected participants (7).
112 In this prior study, we used a support vector machine model with recursive feature elimination to
113 learn patterns of relative abundance of operational taxonomic units (OTUs) that distinguished
114 infected (defined as *Vc* DNA detected in stool, or culture positive) from uninfected persons (*Vc* DNA
115 undetected in stool). The model was trained on a subset of study participants and tested on another
116 subset in a hold-out validation. Here, we have extracted data from this prior study to examine
117 separately the *Pa* OTUs in infected compared to uninfected persons. *Pa* abundance was
118 significantly higher as a proportion of the total sequencing reads in the stool of infected participants
119 (6/22, 27%) of infected household contacts had detectable *Pa* compared to only 5.6% (2/36) of
120 uninfected individuals (Figure 1A). The ratio of *Pa* to *Vc* abundance present during infection was
121 variable and averaged 1:1 (Figure 1B). These findings were particularly interesting because
122 typically there is a drastic reduction of nearly all gut microbes during active *Vc* infection (5, 15) due
123 to secretory diarrhea, oral rehydration solution ingestion, and *Vc* infection itself, and yet here *Pa*
124 was found in an increased abundance in some actively infected participants. Based on these
125 findings, we hypothesized that *Pa* may be resistant to displacement from the gut during infection.
126 While our previous study demonstrates a positive correlation between *Pa* in human stool and *Vc*
127 infection, a causal relationship between this gut microbiota species and *Vc* infection had not been
128 previously established.

129

130 ***Pa* increases *Vc* host colonization**

131 We modified a well-established infant mouse colonization model (18) to assess whether the
132 presence of *Pa* in the small intestine would promote *Vc* host colonization. First, we isolated a

133 spontaneous streptomycin resistant (Strep$^R$) mutant derived from the ATCC type strain of *Pa* for
134 selection and enumeration of *Pa* following host colonization. Infant mice (3-day old) were
135 intragastrically inoculated with *Pa* ($10^7$ colony forming units [CFUs]) every 12 hours for 4 doses (0,
136 12, 24, 36 hours). At 24 and 48 hours after the first inoculation, small intestines from these animals
137 were dissected and homogenized. Gut homogenates were serially diluted and plated on medium
138 containing streptomycin to assess *Pa* colonization. Strep$^R$ *Pa* colonies (>$10^6$ CFUs/small intestine)
139 were recovered at these two time points (Figure 2A), and no Strep$^R$ colonies was detected in the
140 mock treated group, indicating that *Pa* successfully and stably colonized the small intestines of
141 these animals using these methods. Unlike previous studies (9, 10), pretreatment with antibiotics
142 did not change the outcome of *Pa* colonization (not shown). Sequencing analysis of the mouse
143 small intestines demonstrated no significant change in the microbial composition and diversity with
144 and without *Pa* colonization (Supplemental Figure 1 A and B).
145
146 We then evaluated if pre-colonization by *Pa* would influence *Vc* colonization in the small intestine.
147 *Pa* pre-colonization in the infant mice was established over a 36-hour period as described above.
148 Negative control animals were inoculated with sterile media in place of *Pa* over the same dosing
149 schedule. Twelve hours after the last *Pa* inoculation (i.e., 48 hours after the first *Pa* inoculation),
150 these animals were infected with *Vc* ($10^6$ CFU) to evaluate whether pre-colonization with *Pa* had
151 an impact on *Vc* colonization. Although we do not fully understand the exact composition and
152 growth dynamics of *Vc* and *Pa* inside the human gut, the pre-colonization/infection scheme was
153 aimed to closely simulate the ratio of *Pa* to *Vc* observed in the gut microbiota of *Vc* infected humans
154 (Figures 1 and 2A). Comparing *Pa* pre-colonized mice to the control group, there was a significant
155 increase (~10-fold, $p \leq 0.0001$) of *Vc* colonization in the mice pre-colonized with *Pa* (Figure 2B) 24
156 hours after infection. This enhanced intestinal colonization by *Vc* in the *Pa*-colonized mice was

157 observed as early as 6 hours after infection and maintained throughout the colonization period
158 (Supplementary Figure 2).
159
160 We reasoned that it was also possible for *Vc* and *Pa* to encounter one another in the environment
161 before entering the host. To model this scenario, *Vc* was mixed with *Pa* in 1:1 ratio, and the mixture
162 was used immediately for animal infection. In agreement with the results obtained with the *Pa* pre-
163 colonization model, *Vc* intestinal colonization was significantly higher when coinfected with *Pa* than
164 without *Pa* (Figure 2C). Given *Pa* colonization did not overtly change the overall composition of the
165 gut microbiota (Supplementary Figure 1), collectively, our results demonstrate that the presence of
166 a single gut microbiota species is sufficient to increase *Vc* host colonization. Our findings also
167 illustrate that our approach to microbiome studies in humans (6, 7) can be used as a predictive tool
168 to identify gut microbes that alter *Vc* virulence.
169
170 ***Pa* promotes *Vc* biofilm formation**
171 To investigate if the increased *Vc* intestinal colonization is due to direct interactions between *Vc*
172 and *Pa,* these two species were co-cultured and allowed to propagate for three days where both
173 planktonic growth and pellicle formation (i.e., biofilm formation at the air-liquid interface) of both
174 species was monitored. There was a small difference (< 2-fold) in growth in the planktonic phase
175 of either *Vc* or *Pa* in the co-cultures when compared to the cultures containing a single species
176 (Figure 3A). However, the *Vc/Pa* co-culture formed a pellicle that was visibly thicker and more
177 robust than that formed by *Vc* monoculture (photo shown in Figure 3B). The *Pa* monoculture did
178 not form a visible pellicle. The co-culture pellicle samples were carefully lifted and removed from
179 the culture medium, washed, and agitated to release single cells for enumeration of each species.
180 Compared to *Vc* monoculture, the co-culture samples contained over 50-fold more *Vc* cells while
181 the ratio of *Vc* to *Pa* approached to approximately 1:1 (Figure 3C). Moreover, only a small fraction

182 (0.01%) of *Vc* and *Pa* could be washed off from the isolated pellicles (Figure 3D), suggesting that
183 these species are tightly integrated into the pellicle.
184
185 Based on the above data, we hypothesize that *Vc* and *Pa* form dual-species biofilms at the air-
186 liquid interface. This is unexpected because *Vc* is known to form a clonal community in both *in vitro*
187 and *in vivo* biofilms and these are known to exclude other species including even planktonic *Vc*
188 cells (19, 20). To test this hypothesis, we transferred the co-culture pellicles onto coverslips for
189 imaging with confocal microscopy (Figure 4). All cells in the pellicle were stained with FM 4-64
190 membrane dye, and *Vc* cells were differentiated from *Pa* using a constitutively produced
191 mNeonGreen reporter (21) expressed from a neutral *Vc* locus (22). In the *Vc/Pa* co-culture pellicles,
192 we observed a continuous film structure spanning the entire pellicle (Figure 4A). Notably, cocci-
193 shaped *Pa* cells were clearly visible in the co-culture pellicle (Figure 4B-C), consistent with the CFU
194 quantification in Figure 3A. Interestingly, *Pa* cells were found throughout the pellicle, with a higher
195 abundance in the bottom layer (Figure 4D-F), and always in close association with *Vc* cells. In
196 summary, we found that *Vc* and *Pa* coexist stably in the pellicle structure and this relationship may
197 explain the mechanism by which *Pa* resists displacement in humans during active *Vc* infection.
198
199 Next, we used a standard crystal violet (CV) microtiter plate assay (23) to quantitatively evaluate
200 how *Vc* and *Pa* interact under pellicle forming conditions. *Vc* and *Pa* were simultaneously
201 inoculated into the wells of microplates in two different *Vc*:*Pa* ratios (1:1 and 1:10). We also tested
202 if the viability of *Pa* was crucial for this interaction by using heat-killed *Pa* as a control. Consistent
203 with our pellicle compositional analysis, *Vc* formed a more robust biofilm than *Pa* under these
204 conditions as demonstrated by increased CV staining in wells containing *Vc* only compared to wells
205 containing *Pa* only (Figure 5A). Importantly, CV staining was increased in wells containing *Vc* and
206 live *Pa* compared to wells with *Vc* only, in a concentration-dependent manner (Figure 5A). In

207 contrast, CV staining was not different in wells containing *Vc* and heat-killed *Pa* compared to wells
208 with *Vc* only (Figure 5A).
209
210 To replicate our mouse experiments (Figure 2), we also tested if the order in which the two species
211 encounter one another is critical for the *Vc* biofilm enhancement phenotype. *Pa* was grown in wells
212 24 hours before the addition of *Vc*. As in our previous results in the co-inoculation experiment, an
213 increase in CV staining was observed in wells in which the two species were added sequentially,
214 but not in the wells with *Vc* only (Supplementary Figure 3). Moreover, wells pre-incubated with heat-
215 killed *Pa* and subsequently inoculated with *Vc* had no increase in CV staining compared to wells
216 inoculated with *Vc* alone (Supplementary Figure 3). Together, our biofilm quantification data
217 suggests that the presence of *Pa*, regardless of the order of encounter, results in an enhanced
218 biofilm formation of *Vc.*
219
220 ***Vibrio* exopolysaccharide is essential for a stable biofilm structure formed by *Vc* and *Pa***
221 To understand what biofilm component is required for the enhancement of biofilm production in
222 *Vc/Pa* co-culture, we repeated the above experiments with a Δ*vpsL Vc* mutant that cannot produce
223 the *Vibrio* exopolysaccharide (VPS) necessary for mature biofilm formation (24). In contrast to what
224 we observed with a *vpsL*$^{+}$ strain, there was no significant increase in CV staining in wells with both
225 Δ*vpsL* mutants and *Pa*, when compared to wells with the Δ*vpsL* mutants only (Figure 5B).
226
227 To further investigate the role of VPS in promoting co-culture biofilms, we stained the co-culture
228 pellicle *in situ* with Wheat Germ Agglutinin (WGA), a common stain for VPS (which contains GlcNAc
229 moieties, (25)). To avoid spatial overlap with the membrane stain (excited at 561 nm), the *Vc* cells
230 used in this experiment express a cyan-fluorescent protein SCFP3A cytosolically (excited at 445
231 nm), and the WGA is conjugated to Oregon Green (excited at 488 nm). Figure 6A shows a 3D view
232 of a large area of a *Vc/Pa* co-culture pellicle with WGA staining. We then compared the intensity of
233 WGA staining in areas with different compositions of *Vc* and *Pa*. Area 1 in Figure 6A represents a

234 location where *Vc* is the predominant species and *Pa* abundance is low (i.e., FM 4-64 staining
235 overlapped entirely with SCFP3A signal), while areas 2 and 3 in Figure 6A represent locations
236 where *Vc* and *Pa* coexist (i.e., contain regions with FM 4-64 staining but no SCFP3A signal).
237 Surprisingly, the WGA signal intensity was elevated in the *Pa*-rich regions rather than in the *Vc*-
238 rich regions (Figure 6B). Zoom-in view of the *Vc*-enriched region shows the characteristic sub-
239 envelope structures around clusters of *Vc* cells (Figure 6C), consistent with the known VPS
240 morphology in submerged *Vc* biofilms (26). In *Pa*-rich regions, the WGA-signal was stronger, and
241 the VPS structures were more compact (Figure 6C). Importantly, the VPS structure we observed
242 enclose both *Pa* and *Vc* cells, providing an intuitive explanation for how *Pa* cells are incorporated
243 into the pellicle. Together, these results suggested that the physical presence of *Pa* in co-culture
244 pellicle augments the production of VPS in *Vc* cells, leading to increased *Vc* biofilm formation; the
245 *Pa* cells, in turn, rely on VPS to be integrated into the 3D structure of the pellicle.
246
247 **Enhancement of *Vc* host colonization by *Pa* depends on biofilm exopolysaccharide**
248 Biofilm-grown *Vc* cells are known to be more infectious in humans due to increased resistance to
249 gastric pH and higher expression of virulence factors (e.g., such as the toxin co-regulated pilus,
250 which mediates host colonization) compared to planktonically grown cells (27-29). We hypothesize
251 that because *Vc* biofilm formation is enhanced in the presence of *Pa*, this results in increased
252 virulence inside the host, in a VPS-dependent manner.
253
254 To test our hypothesis and measure if the effect of the *Vc/Pa* biofilm interaction impacts host
255 colonization, we compared the colonization efficiency between wild-type (WT) or the Δ*vpsL* mutants
256 in infant mice with and without *Pa* pre-colonization. As shown previously (30), the Δ*vpsL* mutant
257 was able to colonize the mouse small intestine equally as well as the WT *vpsL*$^+$ strain, confirming
258 that the VPS is not absolutely required for host colonization when *Vc* was administered to the
259 animals alone. In contrast, while *Pa* increased WT *vpsL*$^+$ *Vc* colonization, the Δ*vpsL* mutant did not
260 exhibit the enhanced colonization phenotype in the *Pa* pre-colonized mice (Figure 7A). Similar

261 results were observed using the coinfection model; when *Vc* Δ*vpsL* mutants were coinfected with
262 *Pa*, there was no increase in host colonization (Figure 7B). Together, we concluded that the
263 enhancement of *Vc* intestinal colonization in the presence *Pa* is dependent on the *Vibrio*
264 exopolysaccharide, in line with our *in vitro* data.
265
266 **Accessary biofilm matrix proteins are involved in *Pa* and *Vc* interaction**
267 Mature *Vc* biofilm is stabilized with a variety of accessary matrix proteins in addition to the VPS
268 (26, 31, 32). To interrogate the roles of these components in the interactions between *Vc* and *Pa*,
269 we tested mutants lacking the cell-cell adhesion proteins RbmA (26, 31, 33) and mutants lacking
270 surface adhesion redundantly conferred by RbmC and Bap1 (26, 32, 33) for their ability to increase
271 biofilm formation in the presence of *Pa* using CV assays (Figure 7C). When compared to the wells
272 containing the Δ*rbmA* mutant alone, the CV staining was higher in the wells with both the Δ*rbmA*
273 mutant and *Pa.* However, the increase was not as high in the Δ*rbmA* mutant when compared to
274 that in WT *Vc*/*Pa* co-culture (Figure 7C). Furthermore, the presence of *Pa* did not increase CV
275 staining in the wells containing the Δ*rbmC* Δ*bap1* mutants (Figure 7C).
276
277 We then performed the infant mouse colonization experiments with *Vc* biofilm matrix protein
278 mutants using the *Pa* coinfection model to test the roles of these proteins *in vivo*. For this series of
279 experiments, each *Vc* biofilm mutant was coinfected into the animals with *Pa* in 1:1 ratio. In
280 agreement with our *in vitro* results, while host colonization was significantly higher for WT *Vc*
281 coinfected with *Pa* than without *Pa* (Figure 2C), Δ*rbmA* mutants did not show any increase in host
282 colonization when coinfected with *Pa*, and Δ*rbmC* Δ*bap1* mutants demonstrated reduced
283 enhancement in colonization during coinfection with *Pa* (Figure 7B). These results indicate that the
284 ability of *Vc* to form a structurally intact biofilm is important for the enhancement of colonization
285 facilitated by the presence of *Pa.*
286
287

288 **Discussion**

289 Evidence that the composition of the gut microbiota influences the clinical outcomes of enteric
290 infections in humans is accumulating (34, 35). Several studies have identified commensal species
291 and underlying colonization resistance mechanisms that could be protective against *V. cholerae*
292 (*Vc*) infection. While these studies suggest that microbiota species reduce *Vc* virulence through
293 various mechanisms during the early stages of infection (4, 5, 14), the precise role of these
294 colonization resistance mechanisms in impacting susceptibility to cholera in humans has only
295 begun to be appreciated. For instance, a bacterium in the genus *Blautia* was recently found to
296 encode functions that confer colonization resistance (e.g., bile salt hydrolase) to *Vc* infection (4).
297 Consistent with this finding, our previous stool microbiome study has also independently identified
298 that one of the species in the genus *Blautia* is correlated with decreased susceptibility to *Vc*
299 infection (6, 7).

300

301 While previous studies have identified microbiota-associated mechanisms that are protective
302 against *Vc* infection, examples of interactions between *Vc* and a human-associated microbiota
303 species that increases *Vc* pathogenicity are scarce. Although *Escherichia coli* and *Vc* are believed
304 to reside in different intestinal niches, one previous study showed that an atypical *E. coli* isolated
305 from a mouse that does not ferment lactose can increase the virulence of a quorum-sensing (QS)
306 defective *Vc* strain N16961 (36). How QS-proficient *Vc* strains, which are prevalent in toxigenic
307 clinical isolates (37), respond to typical *E. coli* in the human gut remains to be studied. In contrast,
308 a recent study showed that *E. coli* motility facilitates aggregation of these two organisms in a dual-
309 species biofilm, but there was no impact of such aggregation on *Vc* intestinal colonization (38).
310 Indeed, coaggregation between *Vc* and other microbiota species has been observed (39), but these
311 associations are not known to have a direct influence on *Vc* pathogenicity. This is consistent with
312 our prior human studies in which *E. coli* species were present in the gut microbiota of persons
313 during active *Vc* infection, but these were not correlated with active *Vc* infection (7). Our findings
314 highlight the importance of coupling mechanistic studies (*in vitro* and animal models) with human

315 microbiome data analysis to pinpoint the relevant species and interactions involved in enteric
316 infections.
317
318 Here we show that the presence of a human gut microbe *Pa* promotes *Vc* host colonization, which
319 is consistent with our prior human study in which *Pa* was more likely to be present in persons
320 infected with *Vc*. This raises the possibility that uncharacterized interactions between *Vc* and
321 members of the gut microbiota may exacerbate *Vc* virulence and contribute to increased morbidity.
322 Our current study also establishes a plausible mechanism used by *Pa*, and perhaps other gut
323 microbes, to increase the virulence of *Vc* through induction of biofilm formation, a physiological
324 state in which *Vc* is known to increase expression of other virulence factors critical for human
325 infection and disease (27, 28). *Vc* biofilms have also been demonstrated to deform and even
326 damage tissue-engineered soft epithelia mimicking the host tissue (40), suggesting that *in vivo*-
327 formed biofilm structures could negatively impact host gut physiology.
328
329 While VPS and other biofilm components are not usually considered critical host colonization
330 factors, we found that these macromolecular structures were essential for the enhancement of *Vc*
331 host colonization induced by *Pa*. Whether these components mediate other *Vc*-gut microbe
332 interaction has not been studied. Interestingly, many gut microbes appear to predominantly exist
333 in the form of mixed-species biofilms on mucosal surfaces (41), suggesting microbiota-induced
334 biofilm enhancement could play a major role in modulating virulence of other pathogens. Many
335 structural components, regulatory factors, and signaling transduction pathways that control biofilm
336 formation in *Vc* have been well characterized (42), and these factors could be targeted for
337 manipulation by other gut microbes that modulate *Vc* virulence. For example, 3,5-dimethylpyrazin-
338 2-ol (DPO) was recently discovered as a new class of *Vc* quorum-sensing autoinducer that binds
339 to the transcription factor VqmA to activate expression of *vqmR*, which encodes a small regulatory
340 RNA that downregulates *Vc* biofilm formation. The VqmA-VqmR system can be activated both *in*
341 *vitro* by *E. coli* and *in vivo* by *B. obeum* (5, 43), and results in suppression of biofilm formation.

342 Interestingly, *Pa* demonstrates the opposite tendency by promoting *Vc* biofilm formation, with
343 implications for the enhancement of *Vc* colonization, in contrast to other commensal bacteria.
344
345 Many aspects of the *Vc*/*Pa* interaction are still unclear. What is the selective advantage that fosters
346 the formation of dual-species biofilm? Investigation of the structure-function relationship in other
347 multispecies biofilms, such as dental biofilms, demonstrates a coordinated organization of each
348 species that allows for optimal nutrient and oxygen usage, as well as mechanical stability (44, 45).
349 While we did not observe any growth yield enhancement in the planktonic phase of the co-culture,
350 there was a significant increase of *Vc* and *Pa* abundance in the co-culture pellicle at the air-liquid
351 interface. Thus, a possible driving force of this interaction could be the optimization of nutrient
352 sharing and distribution, or removal of toxic metabolites accumulated during growth. The exact
353 mechanism used by these two species to detect and coordinate with each other remains unclear.
354 Secreted small molecules produced by *Pa* do not appear to impact *Vc* as evidenced by our prior
355 studies in which *Vc* cultured in *Pa* spent-cell supernatant did not yield result in increased biofilm
356 formation (7). Therefore, we surmised that the close physical association between *Vc* and *Pa* cells
357 in space in the co-culture pellicles is required for the enhanced biofilm formation. This hypothesis
358 is supported by our microscopy analysis. The *Vc/Pa* interaction has two reciprocal aspects: First,
359 *Pa* activates the production of VPS in *Vc* cells, leading to enhanced pellicle formation. Future
360 characterizations of *Pa* could potentially elucidate the underlying molecular mechanism of this
361 effect *Pa* has on *Vc*. Second, in order to be integrated into the pellicle structure, *Pa* cells seem to
362 physically interact with VPS. Interestingly, we have shown that VPS staining signals are stronger
363 in the *Pa*-rich regions than in the *Vc*-rich regions. This could be explained either by a stronger
364 attraction between VPS and *Pa* than between VPS and *Vc* cells, or by activation of VPS
365 biosynthesis genes in *Vc* cells in the vicinity of the *Pa* cells, or both. Future biochemical and
366 biophysical studies to investigate this relationship may provide new insights about the interactions
367 between *Pa* and *Vc* biofilm, and about pathogen-gut microbe interactions in general. Other
368 members of the *Paracoccus* genus are known to form biofilms and encode adhesins to facilitate

369 surface attachment (46, 47), and the potential role of these adhesins in facilitating interaction with
370 *Vc* remains to be studied.
371
372 In conclusion, we describe a novel interaction between *Vc* and a gut microbe found in high
373 abundance in *Vc*-infected persons that leads to a significant change in *Vc* biofilm behaviors, as well
374 as an increase in the virulence of the pathogen. Our findings are also consistent with other
375 observations that rare gut microbial species can have significant impacts on microbial ecosystems
376 (48). This study adds to the growing number of pathogen-gut microbial species interactions that
377 may impact outcomes in human diseases.
378

379 **Materials and Methods**

380

381 **Prior published study sample collection and analysis**

382 In a prior study, we enrolled household contacts of persons hospitalized with cholera at the
383 International Centre for Diarrheal Disease Research, Bangladesh (icddr,b)(7). Briefly, in this
384 previously published study, household contacts were followed prospectively with rectal swab
385 sampling, 30 days of clinical symptom report, and vibriocidal titer measurements, and 16S rRNA
386 sequencing was performed on rectal swab sampling from the day of enrollment in the study (7).
387 Persons with evidence of *V. cholerae* (*Vc*) infection at the time of enrollment in the study were
388 compared to those who did not have evidence of infection in a model to detect gut microbes that
389 were differentially abundant during *Vc* infection (7). *Vc* infection was defined as *Vc* DNA identified
390 on 16S rRNA sequencing or a positive *Vc* stool culture. In this previously published study, we used
391 a machine learning method called a support vector machine (SVM), which utilizes patterns of OTU
392 relative abundance to detect OTUs associated with infected compared to uninfected persons. This
393 SVM was used with a recursive feature elimination algorithm that simplifies models and increases
394 accuracy of the identification of differentially associated OTUs by removing uninformative bacterial
395 taxa (7). For the present study, we re-examined the microbiome data from household contacts at
396 the time of enrollment to quantify the abundance of 16s rRNA reads that mapped to *Pa* OTUs
397 between uninfected study participants and infected participants.

398

399 **Strains and culture conditions**

400 All *V. cholerae* (*Vc*) strains used in this study are streptomycin-resistant derivatives of C6706, a
401 1991 El Tor O1 clinical isolate from Peru (49). The in-frame Δ*vpsL* deletion mutants used in various
402 assays were previously described (50). The Δ*rbmA* and Δ*rbmC* Δ*bap1* mutants were constructed
403 by allelic exchange (51) using specific suicide vectors described before (20, 52). *Vc* strains used
404 for microscopy experiments, Δ*vc1807*::$P_{tac}$–*mNeonGreen* and Δ*vc1807*::$P_{tac}$ –*SCFP3A-spec*$^{R}$,
405 were constructed using natural transformation as previous described (22). The *P. aminovorans*

406 (*Pa*) used in our experiments is a Strep$^R$ isolate derived from the ATCC type strain (ATCC #49632).
407 *Vc* and *Pa* overnight cultures were grown with aeration in LB at 30°C. Heat-killed strains were
408 incubated at 60°C for 2 hours prior to experimentation. Unless specified, media was supplemented
409 with streptomycin (Sm, 100 µg/ml) and chloramphenicol (Cm, 10 µg/ml) when appropriate.
410

411 **Animal studies**

412 For establishing colonization of the microbiota species, 3-day old suckling CD-1 mice (Charles
413 River Laboratories) were fasted for 1 hour, then orally dosed with *Pa* at a concentration of $10^7$ CFU
414 using 30-gauge plastic tubing, after which the animals were placed with a lactating dam for 10-12
415 hrs and monitored in accordance with the regulations of Tufts Comparative Medicine Services. This
416 inoculation scheme was followed an additional 3 times, for a total of 4 inoculations of *Pa* over the
417 course of 48hrs. After 48hrs, mice were infected with $10^6$ CFU of *Vc*, WT C6706 or mutant strain,
418 or LB as a vehicle control in a gavage volume of 50 µl to evaluate the effect of *Pa* pre-colonization
419 on *Vc* host colonization. At 18-24hrs post-infection, animals were sacrificed, and small intestine
420 tissue samples were collected and homogenized for CFU enumeration. WT *Vc* is *lac*$^+$ and appears
421 blue on medium containing X-gal while *Pa* appears white on the same medium. For coinfection
422 experiments, cultures of *Vc* and *Pa* strains were mixed in a 1:1 ratio and mice were orally dosed
423 with a final bacterial count of $10^6$ CFU. Mice were sacrificed 20-24 hours post-infection and small
424 intestine samples were processed as outlined above to evaluate the colonization efficiency of both
425 species.
426

427 **Ethics Statement**

428 All animal experiments were performed at and in accordance with the rules of the Tufts
429 Comparative Medicine Services (CMS), following the guidelines of the American Veterinary Medical
430 Association (AVMA) as well as the Guide for the Care and Use of Laboratory Animals of the
431 National Institutes of Health. All procedures were performed with approval of the Tufts University
432 CMS (Protocol# B 2018-99). Euthanasia was performed in accordance with guidelines provided by

433 the AVMA and was approved by the Tufts CMS. The previously published study from which Figure
434 1 is derived (7) received approval from the Ethical Review Committee at the icddr,b and the
435 institutional review boards of Massachusetts General Hospital and the Duke University Health
436 System. Participants or their guardians provided written informed consent.
437
438 **Pellicle composition analysis**
439 To assess pellicle composition, overnight cultures of *Vc* and *Pa* were inoculated into glass culture
440 tubes (18 x 150 mm) containing 2mL LB media in a ratio of 1:10 *Vc* ($10^6$) to *Pa* ($10^7$) CFU, and co-
441 cultures were allowed to grow statically at room temperature for 3 days. Following static growth,
442 floating pellicles were carefully transferred into sterile 1.5mL Eppendorf tubes containing 1mL LB,
443 and samples were gently spun down to wash away any planktonic bacteria. Planktonic cells were
444 removed, and cell pellets of pellicle samples were resuspended in 1mL of fresh LB media. All
445 samples including supernatant from the pellicle wash step, were serial diluted and plated on Sm/X-
446 Gal media to differentiate *Vc* (blue) and *Pa* (white) colonies.
447
448 **Crystal violet biomass assays**
449 Crystal violet biofilm assays were performed as described previously in 96-well flat bottom clear,
450 tissue-culture treated polystyrene microplates (ThermoFisher) (23). In each well, *Vc* ($10^6$ CFUs)
451 and/or *Pa* ($10^6$ or $10^7$ CFUs) were inoculated into 200μL of medium. For experiments involving
452 spent culture supernatants, *Vc* ($10^6$ CFUs) were inoculated into each well containing 200 μL of
453 reconditioned supernatants (80% (v/v) filtered spent culture medium and 20% (v/v) 5× LB). Plates
454 were then sealed using a gas permeable sealing film (BrandTech) and incubated at 37°C.
455 Planktonic culture was removed after 24 hours of incubation, plates were washed with distilled
456 water once. Attached biofilms were stained with 0.1% crystal violet at room temperature for 15-20
457 min. The amount of biomass adhered to the sides of each well was quantified by dissolving the
458 crystal violet in 95% ethanol and the absorbance of the resulting solution was measured at 550 nm
459 or 570 nm using a plate reader.

460

461 **Microscopy**

462 Liquid LB culture of *Vc*, *Pa*, and co-cultures (*Pa*:*Vc* = 10:1) were prepared according to procedures
463 described above. To image pellicles, we used a modified literature procedure (53). Monocultures
464 and co-culture pellicles were first prepared following the procedure described above, except that 3
465 mL of the culture was incubated in a 5 mL culture tube. After 3 days of incubation at room
466 temperature, the pellicles were carefully picked up by the large end of a 200 µL pipette tip,
467 transferred to a coverslip (22 x 60 mm, No. 1.5), and immediately covered with another square
468 coverslip to prevent drying. The LB medium contained 4 µg/mL FM 4-64 stain (ThermoFisher) to
469 stain all cells. To stain VPS, the LB medium additionally contained 4 µg/mL of Wheat Germ
470 Agglutinin conjugated to Oregon Green (ThermoFisher). The stained biofilms were imaged with a
471 Nikon-W1 confocal microscope using 60× water objective (numerical aperture = 1.20). The imaging
472 window was 221 × 221 $\mu m^2$. For large-scale view, a 5x5 tiling was performed. For zoom-in view,
473 the *z*-step size was 0.5 µm and the pixel size was 108 nm. For large-scale view, the *z*-step size
474 was 1 µm and the pixel size was 216 nm. The mNeonGreen (or SCFP3A) expressed by *Vc* was
475 imaged at 488 nm (or 445 nm) excitation, FM 4-64 at 561 nm, and WGA-Oregon Green at 488 nm
476 with the corresponding filters. All presented images are raw images processed from Nikon Element
477 software.

478

479 **Statistics**

480 Error bars in the figures depict the median with a 95% confidence interval as indicted. Based on
481 the experimental design, either standard *t*-test or Mann-Whitney test were used to compare
482 treatment groups as indicated in each figure legend.

483

484

485 **Acknowledgments**

486

487 We thank members in the Ng and Weil Labs for helpful discussions. We acknowledge Ed Ryan for
488 his assistance in reviewing the manuscript. A.A.W and W-L.N. received support from a Rozan
489 Award from Tufts University School of Medicine for this project. A.A.W. support was provided by
490 AI123494 from the National Institute of Allergy and Infectious Diseases (NIAID). W-L.N was
491 supported by AI121337. J.Y. holds a Career Award at the Scientific Interface from the Burroughs
492 Wellcome Fund.
493
494
495

496 **References**


497 1. Camacho A*, et al.* (2018) Cholera epidemic in Yemen, 2016-18: an analysis of
498 surveillance data. *Lancet Glob Health* 6(6):e680-e690.

499 2. Luquero FJ*, et al.* (2016) Mortality Rates during Cholera Epidemic, Haiti, 2010-
500 2011. *Emerg Infect Dis* 22(3):410-416.

501 3. Weil AA & Ryan ET (2018) Cholera: recent updates. *Curr Opin Infect Dis*
502 31(5):455-461.

503 4. Alavi S*, et al.* (2020) Interpersonal Gut Microbiome Variation Drives Susceptibility
504 and Resistance to Cholera Infection. *Cell* 181(7):1533-1546.e1513.

505 5. Hsiao A*, et al.* (2014) Members of the human gut microbiota involved in recovery
506 from *Vibrio cholerae* infection. *Nature* 515(7527):423-426.

507 6. Levade I*, et al.* (2020) Predicting *Vibrio cholerae* infection and disease severity
508 using metagenomics in a prospective cohort study. *J Infect Dis*.

509 7. Midani FS*, et al.* (2018) Human Gut Microbiota Predicts Susceptibility to *Vibrio*
510 *cholerae* Infection. *J Infect Dis*.

511 8. McKenney PT & Pamer EG (2015) From Hype to Hope: The Gut Microbiota in
512 Enteric Infectious Disease. *Cell* 163(6):1326-1332.

513 9. Freter R (1955) The fatal enteric cholera infection in the guinea pig, achieved by
514 inhibition of normal enteric flora. *J Infect Dis* 97(1):57-65.

515 10. Nygren E, Li BL, Holmgren J, & Attridge SR (2009) Establishment of an Adult
516 Mouse Model for Direct Evaluation of the Efficacy of Vaccines against *Vibrio*
517 *cholerae*. *Infection and Immunity* 77(8):3475.

518 11. Zhao W, Caro F, Robins W, & Mekalanos JJ (2018) Antagonism toward the
519 intestinal microbiota and its effect on *Vibrio cholerae* virulence. *Science*
520 359(6372):210-213.

521 12. Jung SA, Chapman CA, & Ng WL (2015) Quadruple quorum-sensing inputs control
522 *Vibrio cholerae* virulence and maintain system robustness. *PLoS Pathog*
523 11(4):e1004837.

524 13. Watve S*, et al.* (2020) Parallel quorum-sensing system in *Vibrio cholerae* prevents
525 signal interference inside the host. *PLoS Pathog* 16(2):e1008313.

526 14. You JS*, et al.* (2019) Commensal-derived metabolites govern *Vibrio cholerae*
527 pathogenesis in host intestine. *Microbiome* 7(1):132.

528 15. David LA*, et al.* (2015) Gut microbial succession follows acute secretory diarrhea
529 in humans. *mBio* 6(3):e00381-00315.

530 16. Yatsunenko T*, et al.* (2012) Human gut microbiome viewed across age and
531 geography. *Nature* 486(7402):222-227.

532 17. Urakami T, Araki H, Oyanagi H, Suzuki K, & Komagata K (1990) *Paracoccus*
533 *aminophilus* sp. nov. and *Paracoccus aminovorans* sp. nov., which utilize N,N-
534 dimethylformamide. *International journal of systematic bacteriology* 40(3):287-291.

535 18. Klose KE (2000) The suckling mouse model of cholera. *Trends Microbiol* 8(4):189-
536 191.

537 19. Millet YA*, et al.* (2014) Insights into *Vibrio cholerae* intestinal colonization from
538 monitoring fluorescently labeled bacteria. *PLoS Pathog* 10(10):e1004405.

539 20. Nadell CD, Drescher K, Wingreen NS, & Bassler BL (2015) Extracellular matrix
540 structure governs invasion resistance in bacterial biofilms. *ISME J* 9(8):1700-1709.

541 21. Shaner NC*, et al.* (2013) A bright monomeric green fluorescent protein derived
542 from *Branchiostoma lanceolatum*. *Nat Methods* 10(5):407-409.

543 22. Dalia AB, McDonough E, & Camilli A (2014) Multiplex genome editing by natural
544 transformation. *Proc Natl Acad Sci U S A* 111(24):8937-8942.

545 23. O'Toole GA (2011) Microtiter dish biofilm formation assay. *J Vis Exp* (47).

546 24. Yildiz FH & Schoolnik GK (1999) *Vibrio cholerae* O1 El Tor: identification of a gene
547 cluster required for the rugose colony type, exopolysaccharide production, chlorine
548 resistance, and biofilm formation. *Proc Natl Acad Sci U S A* 96(7):4028-4033.

549 25. Yildiz F, Fong J, Sadovskaya I, Grard T, & Vinogradov E (2014) Structural
550 characterization of the extracellular polysaccharide from *Vibrio cholerae* O1 El-Tor.
551 *PLoS One* 9(1):e86751.

552 26. Berk V*, et al.* (2012) Molecular architecture and assembly principles of *Vibrio*
553 *cholerae* biofilms. *Science* 337(6091):236-239.

554 27. Tamayo R, Patimalla B, & Camilli A (2010) Growth in a biofilm induces a
555 hyperinfectious phenotype in *Vibrio cholerae*. *Infect Immun* 78(8):3560-3569.

556 28. Gallego-Hernandez AL*, et al.* (2020) Upregulation of virulence genes promotes
557 *Vibrio cholerae* biofilm hyperinfectivity. *Proc Natl Acad Sci U S A* 117(20):11010-
558 11017.

559 29. Zhu J & Mekalanos JJ (2003) Quorum sensing-dependent biofilms enhance
560 colonization in *Vibrio cholerae*. *Dev Cell* 5(4):647-656.

561 30. Fong JCN, Syed KA, Klose KE, & Yildiz FH (2010) Role of Vibrio polysaccharide
562 (*vps*) genes in VPS production, biofilm formation and *Vibrio cholerae*
563 pathogenesis. *Microbiology (Reading)* 156(Pt 9):2757-2769.

564 31. Fong JC, Karplus K, Schoolnik GK, & Yildiz FH (2006) Identification and
565 characterization of RbmA, a novel protein required for the development of rugose
566 colony morphology and biofilm structure in *Vibrio cholerae*. *J Bacteriol*
567 188(3):1049-1059.

568 32. Fong JC & Yildiz FH (2007) The *rbmBCDEF* gene cluster modulates development
569 of rugose colony morphology and biofilm formation in *Vibrio cholerae*. *J Bacteriol*
570 189(6):2319-2330.

571 33. Absalon C, Van Dellen K, & Watnick PI (2011) A communal bacterial adhesin
572 anchors biofilm and bystander cells to surfaces. *PLoS Pathog* 7(8):e1002210.

573 34. Ubeda C, Djukovic A, & Isaac S (2017) Roles of the intestinal microbiota in
574 pathogen protection. *Clinical & Translational Immunology* 6(2):e128.

575 35. Weil AA, Becker RL, & Harris JB (2019) *Vibrio cholerae* at the Intersection of
576 Immunity and the Microbiome. *mSphere* 4(6):e00597-00519.

577 36. Yoon MY*, et al.* (2016) A single gene of a commensal microbe affects host
578 susceptibility to enteric infection. *Nat Commun* 7:11606.

579 37. Wang Y*, et al.* (2011) The Prevalence of Functional Quorum-Sensing Systems in
580 Recently Emerged *Vibrio cholerae* Toxigenic Strains. *Environ Microbiol Rep*
581 3(2):218-222.

582 38. Wang H*, et al.* (2021) Contributions of *Escherichia coli* and its motility to the
583 formation of dual-species biofilms with *Vibrio cholerae*. *Appl Environ*
584 *Microbiol*:AEM0093821.

585 39. Toh YS*, et al.* (2019) Role of coaggregation in the pathogenicity and prolonged
586 colonisation of *Vibrio cholerae*. *Med Microbiol Immunol* 208(6):793-809.

587 40. Cont A, Rossy T, Al-Mayyah Z, & Persat A (2020) Biofilms deform soft surfaces
588 and disrupt epithelia. *Elife* 9:e56533.

589 41. Sadiq FA*, et al.* (2021) Synergistic interactions prevail in multispecies biofilms
590 formed by the human gut microbiota on mucin. *FEMS Microbiol Ecol* 97(8).

591 42. Teschler JK*, et al.* (2015) Living in the matrix: assembly and control of *Vibrio*
592 *cholerae* biofilms. *Nat Rev Microbiol* 13(5):255-268.

593 43. Papenfort K*, et al.* (2017) A *Vibrio cholerae* autoinducer-receptor pair that controls
594 biofilm formation. *Nat Chem Biol* 13(5):551-557.

595 44. Christensen BB, Haagensen JA, Heydorn A, & Molin S (2002) Metabolic
596 commensalism and competition in a two-species microbial consortium. *Appl*
597 *Environ Microbiol* 68(5):2495-2502.

598 45. Mark Welch JL, Rossetti BJ, Rieken CW, Dewhirst FE, & Borisy GG (2016)
599 Biogeography of a human oral microbiome at the micron scale. *Proc Natl Acad Sci*
600 *U S A* 113(6):E791-800.

601 46. Yoshida K, Toyofuku M, Obana N, & Nomura N (2017) Biofilm formation by
602 *Paracoccus denitrificans* requires a type I secretion system-dependent adhesin
603 BapA. *FEMS Microbiol Lett* 364(4).

604 47. Srinandan CS, Jadav V, Cecilia D, & Nerurkar AS (2010) Nutrients determine the
605 spatial architecture of *Paracoccus* sp. biofilm. *Biofouling* 26(4):449-459.

606 48. Jousset A*, et al.* (2017) Where less may be more: how the rare biosphere pulls
607 ecosystems strings. *ISME J* 11(4):853-862.

608 49. Thelin KH & Taylor RK (1996) Toxin-coregulated pilus, but not mannose-sensitive
609 hemagglutinin, is required for colonization by *Vibrio cholerae* O1 El Tor biotype
610 and O139 strains. *Infect Immun* 64(7):2853-2856.

611 50. Waters CM, Lu W, Rabinowitz JD, & Bassler BL (2008) Quorum sensing controls
612 biofilm formation in *Vibrio cholerae* through modulation of cyclic di-GMP levels and
613 repression of *vpsT*. *J Bacteriol* 190(7):2527-2536.

614 51. Skorupski K & Taylor RK (1996) Positive selection vectors for allelic exchange.
615 *Gene* 169(1):47-52.

616 52. Yan J, Sharo AG, Stone HA, Wingreen NS, & Bassler BL (2016) *Vibrio cholerae*
617 biofilm growth program and architecture revealed by single-cell live imaging. *Proc*
618 *Natl Acad Sci U S A* 113(36):E5337-5343.

619 53. Fiebig A (2019) Role of Caulobacter Cell Surface Structures in Colonization of the
620 Air-Liquid Interface. *J Bacteriol* 201(18).

621

622

623 **Figures and Tables**

624

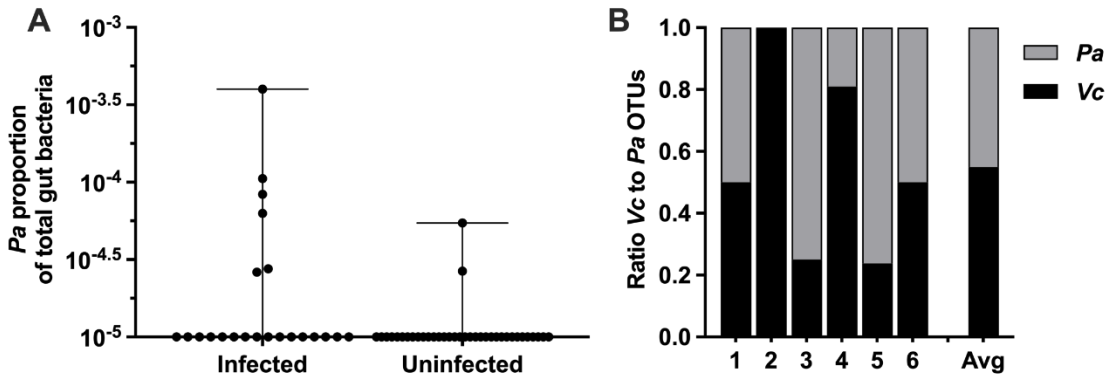


625

626

627 **Figure 1. *Pa* is more abundant in persons with *Vc* infection compared to**

628 **uninfected persons.** In a prior study of household contacts of cholera patients in

629 Bangladesh (7), *Pa* was identified as differentially abundant using a support vector

630 machine model with recursive feature elimination in order to discriminate patterns of

631 microbial taxa relative abundance that distinguished infected from uninfected persons.

632 The microbiota was assessed using 16S rRNA in rectal swabs collected from individuals

633 with *Vc* infection ($n$ = 22) compared to uninfected individuals ($n$ = 36). In this study, total

634 sum normalization was applied to OTU counts from each sample, and a median of

635 37,958 mapped reads per sample were generated (7). Based on this sequencing data,

636 the estimated limit of detection for a *Pa* OTU is $2.0 \times 10^{-5}$. **(A)** Relative abundance *Pa* in

637 infected and uninfected individuals and **(B)** ratio of *Vc* to *Pa* in six *Vc*-infected persons.

638 All data points are shown and boxes indicate interquartile range. Bars mark the

639 maximum and minimum values. These values were compared with non-parametric

640 unpaired Mann-Whitney U testing, $P < 0.01$.

641 .

642

643

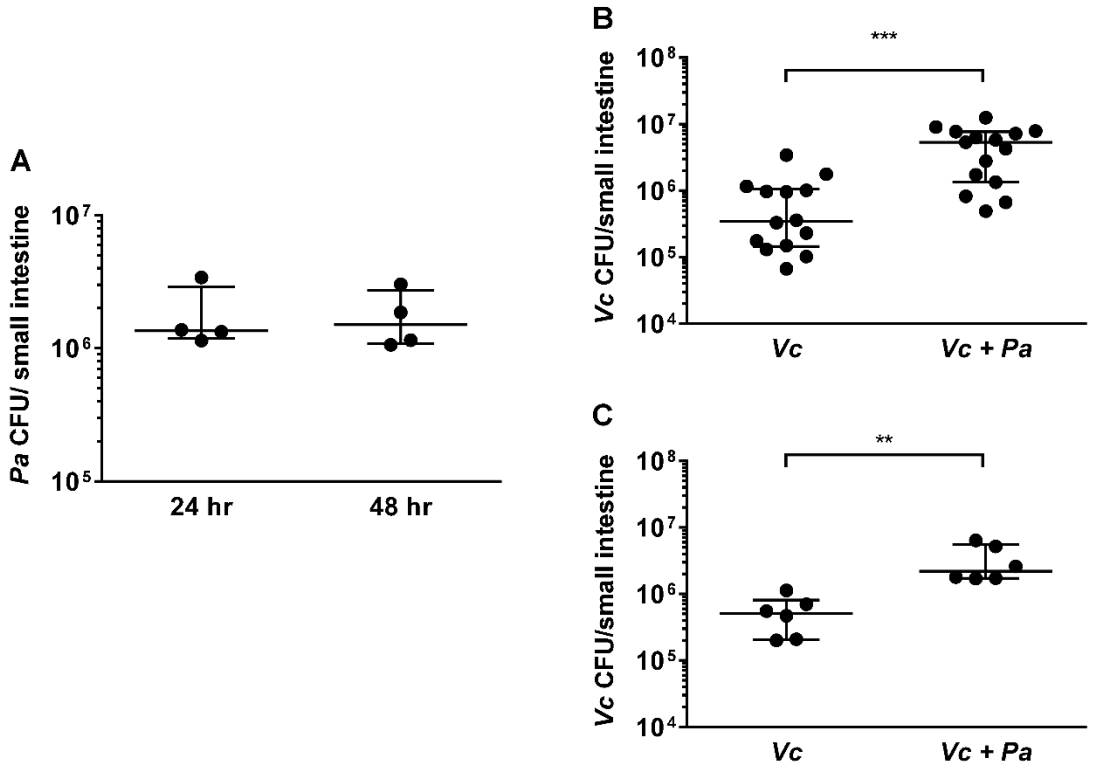


644

645 **Figure 2. The presence of *Pa* enhances *Vc* colonization in the infant mouse**
646 **intestine. (A)** 3 day-old infant mice were intragastrically inoculated with $10^7$ CFU of *Pa*
647 every 12 hours for a period of 24 hr (2 doses) or 48 hr (4 doses). At each time point mice
648 were sacrificed and CFU were enumerated by plating serial dilutions of small intestine
649 samples on selective media. **(B)** 3 day-old infant mice were intragastrically inoculated 4
650 times with LB or $10^7$ CFU of *Pa* for every 12 hours, and subsequently infected with $10^6$
651 CFU of WT *Vc.* Mice were sacrificed 20-24 hr post-infection and the small intestine
652 samples were taken to enumerate *Vc*. Bars on graphs depict median value with 95%
653 confidence interval (CI) and individual data points plotted. Unpaired non-parametric *t*-test
654 (Mann-Whitney); *** $P \leq 0.0001$. (C) *Vc* was inoculated intragastrically into the animals
655 alone or together with *Pa* in a 1:1 ratio. After 24 hours, enumeration of *Vc* was

656 performed as described above. Unpaired non-parametric *t*-test (Mann-Whitney); ** $P \leq$

657 0.005.

658

659

660

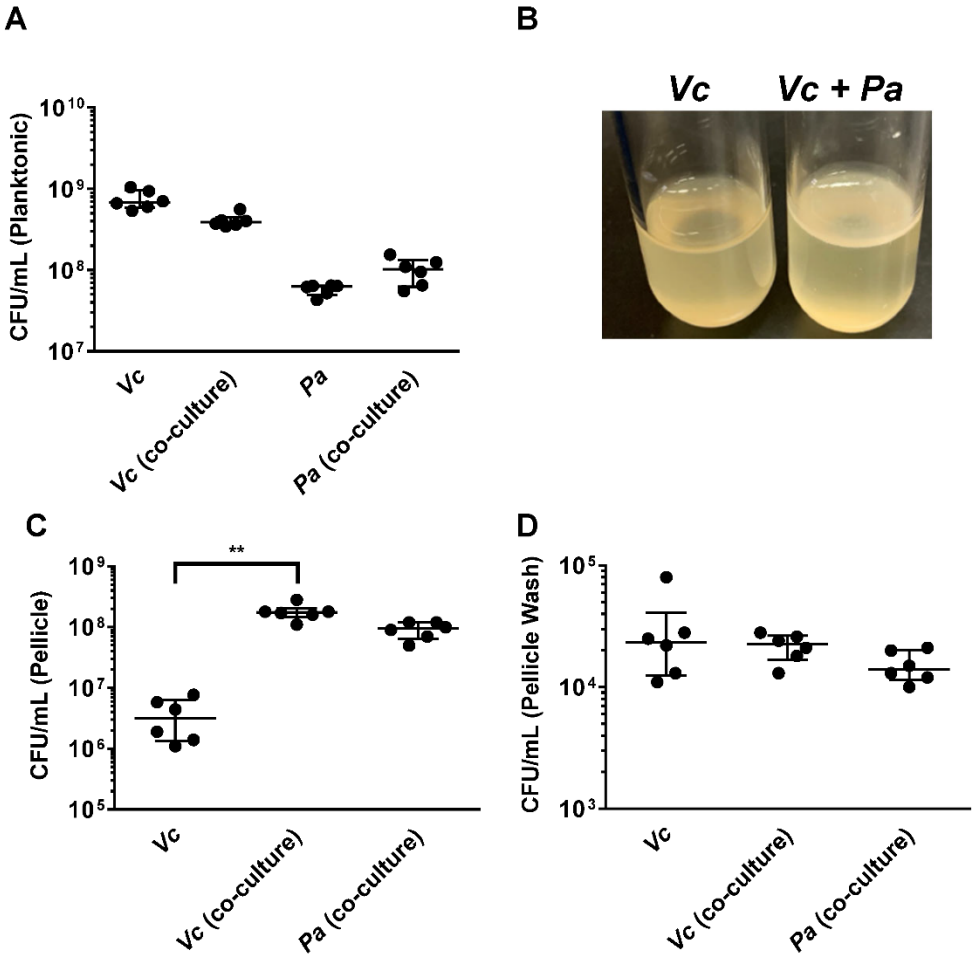


**Figure 3. *Pa* promotes biofilm formation of *Vc*. (A)** Planktonic cell counts from cultures used for pellicle analysis of *Vc* and *Pa* grown together or in monoculture. **(B)** Representative images of pellicles formed by *Vc* grown in monoculture and in co-culture with *Pa*. CFU counts of each strain in **(C)** pellicle samples and **(D)** spent medium used to wash the pellicle. Bars on graphs depict median value with 95% confidence interval (CI) and individual data points plotted. Unpaired non-parametric *t*-test (Mann-Whitney): ** $P \leq 0.005$.

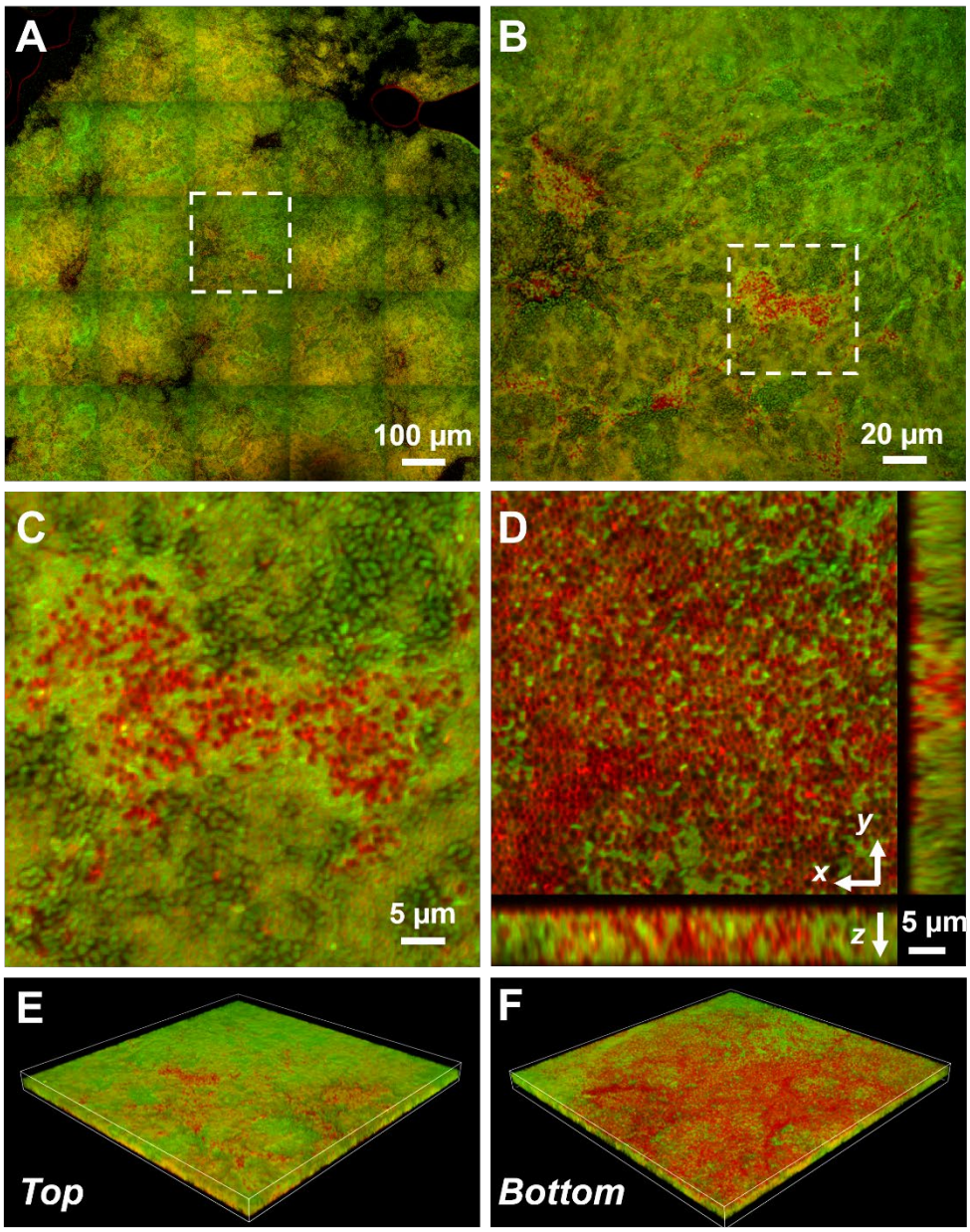


**Figure 4. Representative microscopy images of *Vc* and *Pa* dual-species pellicles.** **(A)** Large-scale cross-sectional image of the internal structure in a co-culture pellicle. All cells are stained with FM 4-64 and *Vc* cells constitutively express mNeonGreen. Therefore, the red signal in the overlay image corresponds primarily to *Pa* cells. **(B)** Zoom-in view of the region highlighted in A. **(C)** Zoom-in view of the region highlighted in B. **(D)** Cross-sectional views of the region shown in C, at the bottom of the pellicle. *Pa*

677 cells exist mainly at the pellicle-liquid interface, with clusters of *Pa* cells penetrating into

678 the interior of the pellicle. **(E-F)** *Top* (E) and *Bottom* (F) view of the co-culture structure

679 shown in B, rendered in 3D.

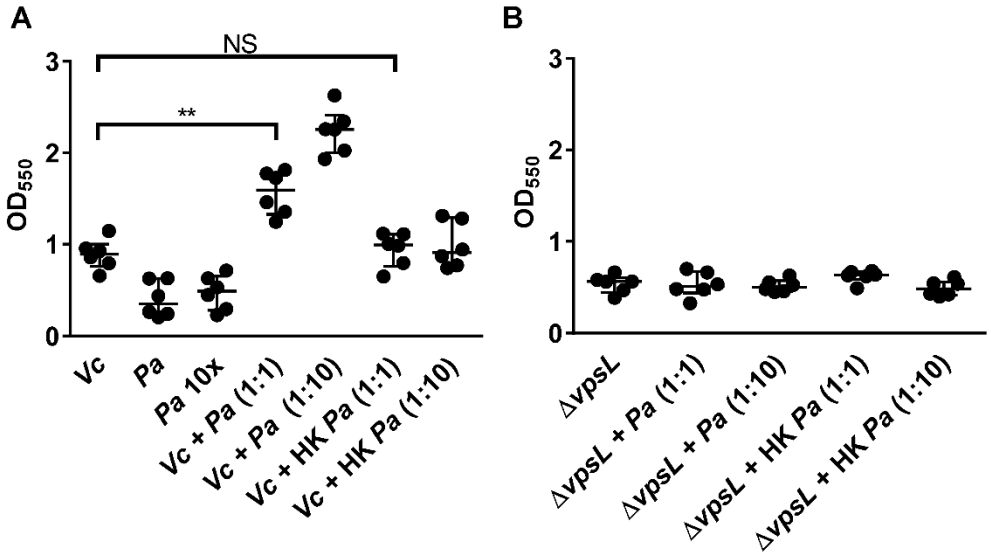


680

681 **Figure 5. *Pa* increases biofilm production in *Vc*.** Crystal violet assays were performed
682 in 96-well microtiter plates to quantify biofilm formation. Overnight-grown **(A)** wild-type
683 *Vc* or **(B)** Δ*vpsL* mutant and *Pa* cultures were diluted to a final concentration of $10^6$ CFU
684 in a total volume of 200 µL/well. In samples containing a 1:10 ratio of *Vc*/*Pa*, *Pa* was
685 diluted to a final concentration of $10^7$ CFU. Samples with heat-killed (HK) *Pa* are
686 specified in the x-axis. Microtiter plates were incubated at 37 °C for 24 hr. Crystal violet
687 staining and ethanol solubilization were performed as previously described (23).
688 Absorbance of the crystal violet stain was measured at 550 nm using a Biotek Synergy
689 HTX plate reader. Data is represented with horizontal lines indicating the mean with
690 standard deviation. Unpaired *t*-test (Mann-Whitney); $^{**}P \leq 0.005$.

691

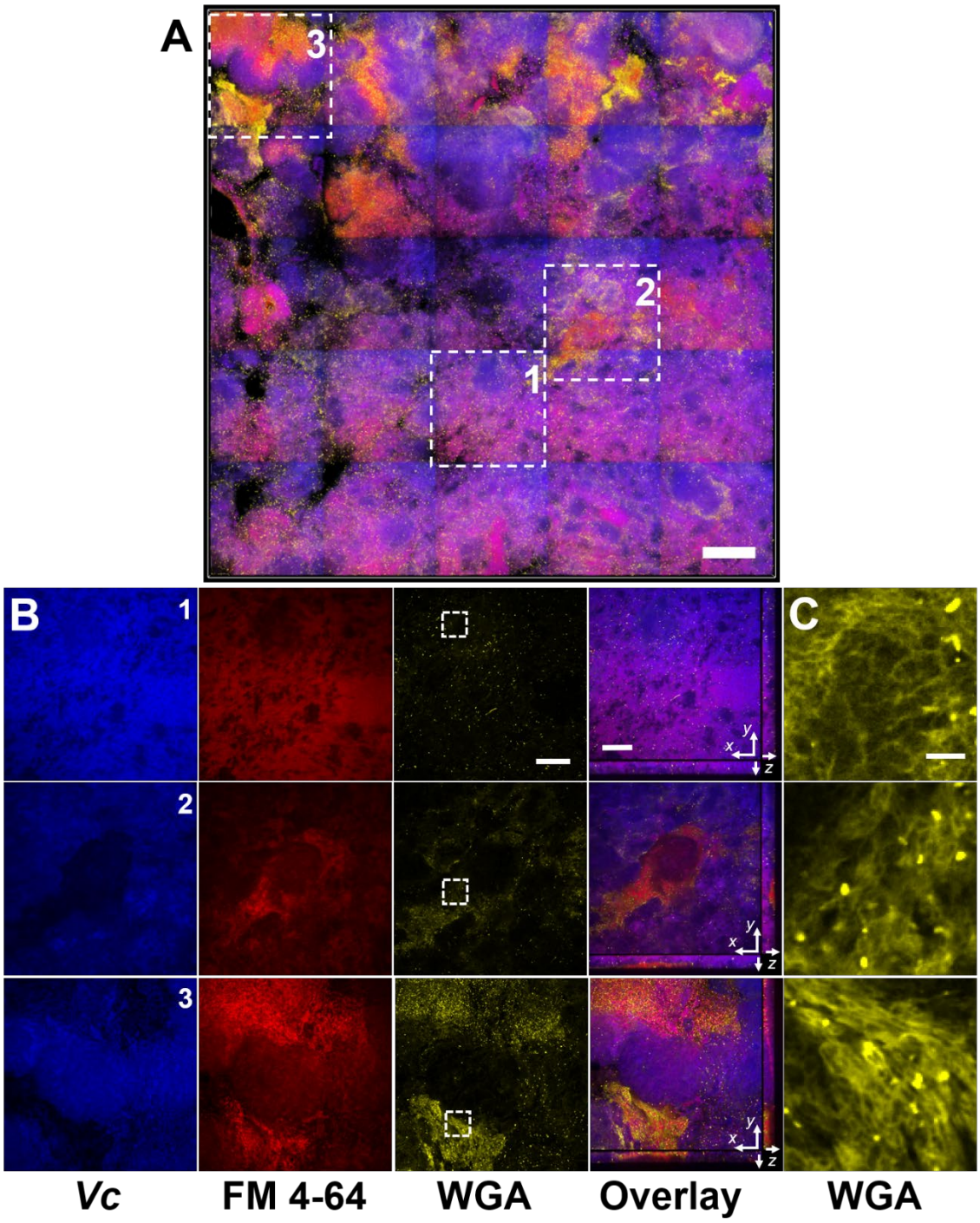


692

693 **Figure 6. *Vc*/*Pa* co-culture biofilms depend on VPS. (A)** Representative top view of a

694 co-culture pellicle with WGA staining, rendered in 3D. *Vc* cells constitutively express

695 SCFP3A cytosolically; all cells were stained with FM 4-64 membrane stain; WGA is

696 conjugated to Oregon Green and shown in yellow. Note that WGA also stained dead
697 cells with an exposed peptidoglycan layer, corresponding to the bright spots in the
698 image. Scale bar: 100 μm. **(B)** Zoom-in view of the three regions 1-3 indicated by the
699 white boxes in A. Shown from *left* to *right* are *Vc* cell fluorescence (SCFP3A), membrane
700 staining (FM 4-64), WGA staining (Oregon Green), and the overlay of the three
701 channels. The overlaid images additionally show the cross-sectional view in the *xz* and
702 *yz* planes. Region 1 contains primarily *Vc* cells, and regions 2 and 3 contain *Pa*-enriched
703 regions. *Pa*-enriched regions demonstrate elevated WGA signal. Intensities in each
704 channel were kept consistent through region 1-3 for comparison. Scale bars: 20 μm. **(C)**
705 Zoom-in view of the highlighted regions in B (white boxes, WGA channel only).
706 Intensities are adjusted to similar level for visualization of the internal structure. Scale
707 bar: 5 μm.
708
709

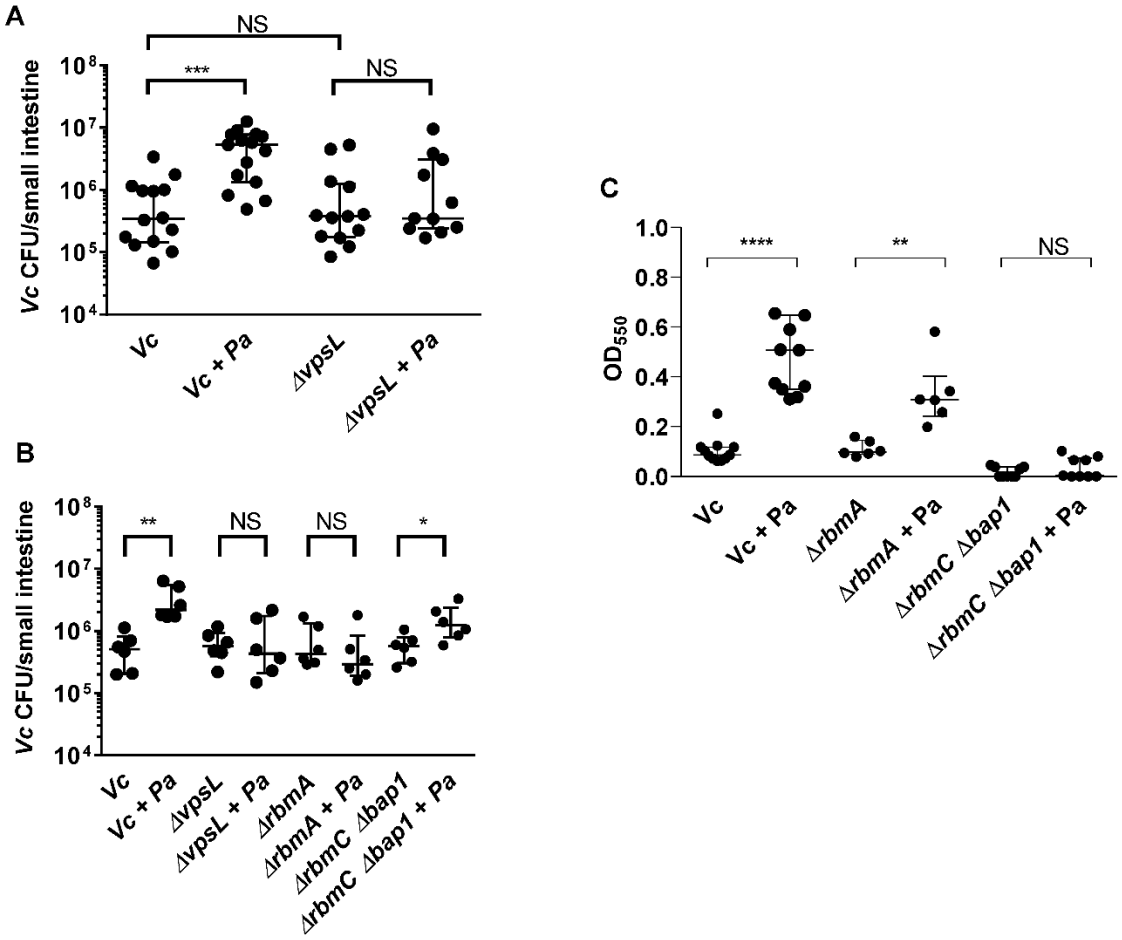


710

711 **Figure 7. Enhanced *Vc* intestinal colonization in the presence of *Pa* is dependent**
712 **on VPS and accessory matrix proteins. (A)** 3 day-old infant mice were intragastrically
713 inoculated with LB or $10^7$ CFU of *Pa* every 12 hours for a period of 48 hours, and
714 subsequently infected with $10^6$ CFU of a *Vc* strain defective for extracellular matrix
715 production (Δ*vpsL*). Mice were sacrificed 20-24 hr post-infection and small intestine
716 samples were taken to enumerate *Vc* CFU. Data from infection with the wild-type *Vc*
717 strain (Figure 2B) is shown again here for comparison purposes. **(B)** *Vc* wild-type (WT)
718 or different biofilm mutants were mixed with *Pa* in 1:1 ratio, and the mixture was used
719 immediately for animal infection. Mice were sacrificed 20-24 hr post-infection and small
720 intestine samples were taken to enumerate *Vc* CFU. Each symbol represents an

721 individual mouse and data is represented with horizontal lines indicating the median with
722 a 95% confidence interval. Unpaired non-parametric *t*-test (Mann-Whitney); ns $P > 0.05$,
723 *** $P \leq 0.001$. Data from infection with the wild-type *Vc* strain (Figure 2C) is shown again
724 here for comparison purposes. **(C)** Crystal violet assays performed in 96-well plates to
725 quantify pellicle formation. Overnight cultures of *Vc rbmA*$^{-}$*, rbmC*$^{-}$ *bap1*$^{-}$ and *Pa* were
726 diluted in fresh LB and plated as 200 µL/well. Samples were co-cultured in either 1:10
727 ratios of Vc/Pa and incubated at 37 °C for 24 hr. Crystal violet staining was then
728 performed and absorbance of the stain was measured at 570 nm. Horizontal lines
729 indicating mean with standard deviation are shown. Unpaired *t*-test; ****$P \leq 0.0001$, **$P$
730 $\leq 0.05$.
731

732 **Supplemental Figures**

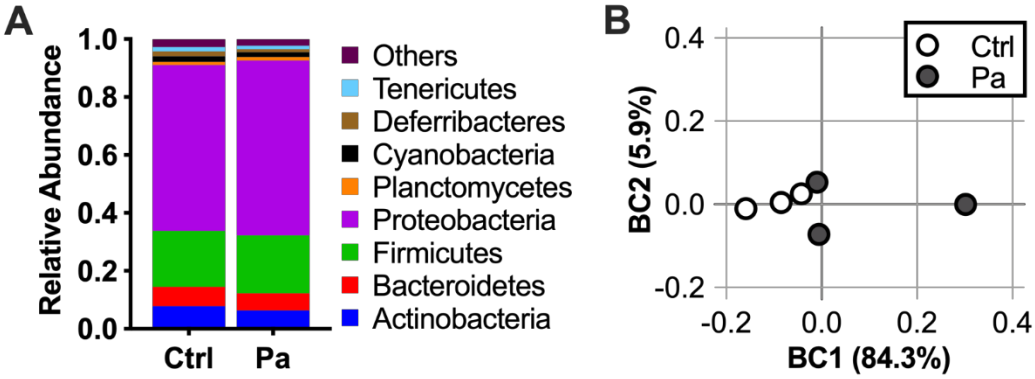


733

734 **Supplemental Figure 1. *P. aminovorans* colonization does not significantly alter**
735 **the mouse gut microbial diversity.** Three day-old infant mice were intragastrically
736 inoculated with $10^7$ CFU of *Pa* or sterile LB medium as control (Ctrl) for a period of 12
737 hours to mimic the length of time between the final *Pa* inoculation and *Vc* infection in
738 mouse experiments. Small intestines were removed, homogenized, and DNA was
739 extracted and sequenced using shallow shotgun sequencing. **(A)** Relative abundance of
740 phylum-level microbes in the small intestines of mice and **(B)** principal component of
741 analysis using Bray Curtis Dissimilarity. N=3 per group. *Pa* is in the Proteobacteria
742 phylum. Two-way ANOVA testing of phylum level-abundance was performed, and all
743 comparisons are not significantly different (P>0.05).

744

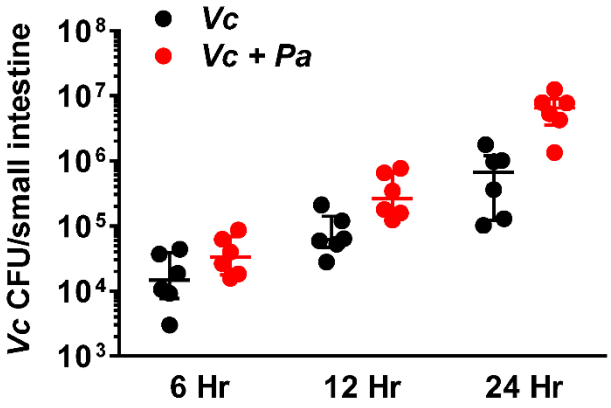


745

746 **Supplemental Figure 2. *P. aminovorans* (*Pa*) colonization significantly increases *V.***
747 ***cholerae* (*Vc*) small intestine colonization.** Three day-old infant mice were
748 intragastrically inoculated with $10^7$ CFU of *Pa* or sterile LB medium as control for a
749 period of 36 hours. These animals were then infected with *Vc* 48 hours after the first
750 inoculation. At different time points, small intestines were removed, homogenized, and
751 *Vc* were enumerated. Student t-tests were used to analyze these samples. P values are
752 0.14, 0.035, and 0.004 at 6, 12, and 24 hours respectively (Unpaired non-parametric *t*-
753 test).

754

755

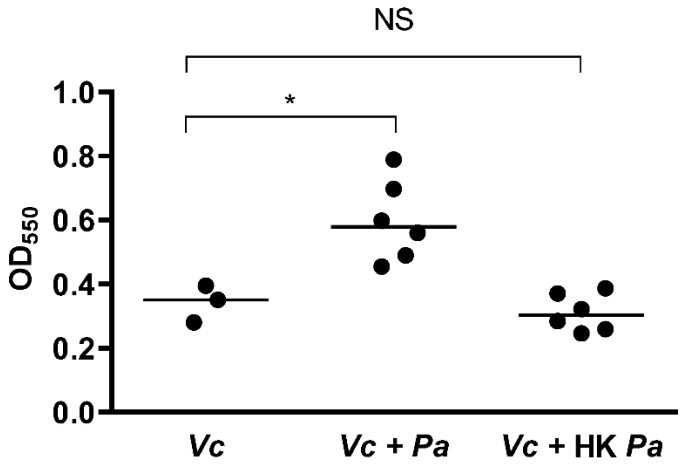


756
757
758 **Supplemental Figure 3. Established *Pa* cultures increase biofilm production in *Vc*.**
759 Biofilm formation assays were performed in 96-well microtiter plates. *Pa* was diluted in
760 LB to a concentration of $10^7$ CFU and grown for 24hr before the addition of WT *Vc*. WT
761 *Vc* was then diluted in LB to a concentration of $10^6$ CFU and added to wells. Plates were
762 incubated for an additional 24hr before crystal violet staining to quantify biofilm biomass.
763 Crystal violet staining and ethanol solubilization were performed as previously described
764 (23). Absorbance of the crystal violet stain was measured at 550 nm using a Biotek
765 Synergy HTX plate reader. Samples with heat-killed (HK) *Pa* are delineated by hatched
766 bars. Data is represented with horizontal lines indicating the median with 95%
767 confidence interval. Unpaired non-parametric t-test (Mann-Whitney); * $P \leq 0.05$.
768

769